A Systematic Study of Structures, Stability, and Electronic Properties of alloy clusters $AlBe_n$ (n = 1–12): Comparison with Pure Beryllium Clusters

Dan Yu[1], Wei-Ming Sun[2], Jing-yao Liu[3], Wu Di[1], Ying Li[3], and Zhi-Ru Li[3]

[1]Jilin University
[2]Department of Basic Chemistry, The School of Pharmacy, Fujian Medical University
[3]Institute of theoretical chemistry Jilin University

September 16, 2020

Abstract

The geometric structures, energetic and electronic properties of global minima of the $AlBe_n$ (n = 1–12) clusters have been systemically studied by using the hybrid density functional theory [B3LYP] and coupled cluster [CCSD(T)] methods. It is found that the impurity Al atom is externally bound to the host Ben framework and its maximum coordination number is six. Besides, the geometries of $AlBe_n$ bear close resemblance to either local or global minimum structures of Be_{n+1}. The $AlBe_3$ and $AlBe_8$ clusters exhibit high relative stability among the $AlBe_n$ clusters, which is reflected by the evolutions of average atomic binding energy, dissociation energy, second difference in energy, adsorption energy of Al, and HOMO-LUMO gap with cluster size. In comparison to the pure Be_{n+1} clusters, $AlBe_n$ exhibit larger binding energy values, whereas they are more polarizable.

A Systematic Study of Structures, Stability, and Electronic Properties of alloy clusters $AlBe_n$ (n = 1–12): Comparison with Pure Beryllium Clusters

Dan Yu, 11*Institute of Theoretical Chemistry, Jilin University, Changchun 130023, (P. R. China)***Wei-Ming Sun,** 22*The School of Pharmacy, Fujian Medical University, Fuzhou 350108, (P. R. China)* **Jing-Yao Liu,[1] Di Wu,[1] Ying Li,[1] and Zhi-Ru Li[1]**

Correspondence to: Wei-Ming Sun (E-mail:*sunwm@fjmu.edu.cn*); Ying Li (E-mail: *liyingedu@jlu.edu.cn*)

Introduction

As a bridge between atoms and macroscopic state, cluster science continues to be a subject of increasing research interest. In the realm of cluster investigations, metal clusters[1–7]have attracted extensive attention in the last several decades because they exhibit many intriguing properties that are neither atomic-like nor extended solidlike,[8,9] while being closely connected to size, geometry, and composition. These size-dependent properties offer exciting possibilities for developing finely tuned cluster-assembled materials, which have promising applications in the fields of material science, optics, nanotechnology, catalysis, etc.[10–14]Besides, it has long been recognized that the properties of metal clusters, instead of evolving linearly with size, usually vary discontinuously with the number of component atoms.[11] In this respect, a simple yet helpful free-electron model, namely spherical jellium model (SJM),[15] has been proposed to account for the evolution of properties (even structures) of numerous pure and doped metal clusters.[16,17]

The fact that beryllium dimer is weakly bound[18–22] whereas bulk beryllium is a hard metal with rather high melting point and enthalpy of atomization[23] makes beryllium cluster an ideal prototype for exploring the evolution from discrete molecules to metallic state, as indicated in an overview on the studies of beryllium

clusters.[24] In contrast to experimental studies which are limited by the toxicity of beryllium, quantum chemistry provides powerful computational methods that help to investigate beryllium clusters in detail. By using density functional theory with Becke–Lee–Yang–Parr gradient correction, Wang et al.[25] studied the structural and electronic properties of beryllium clusters containing up to 21 atoms, and they found that the Be_4, Be_{10} and Be_{17} clusters show particularly high stability. With the help of a modified genetic algorithm, Khanna and coworkers[26] have revealed the dependence of relative stability and electronic properties of the Be_n (n = 2 - 41) clusters on their equilibrium geometries.

Recently, doped metal clusters have attracted much attention from both theoretical and experimental researchers. It has been found that the characteristics of pure metal clusters, such as relative stability, structural evolution, bonding character, electronic and magnetic properties, etc., are usually altered when a heteroatom is introduced. Consequently, doped clusters may show new physicochemical properties not found in pure clusters. In this study, we focus on doped beryllium clusters and choose Al atom as the dopant atom. On the one hand, impurity-atom doping may provide additional flexibility to modulate the physical and chemical properties of beryllium clusters. On the other hand, the systematical study of beryllium-aluminum binary clusters is a meaningful project in view of the important applications of Be-Al alloys in disk drive armatures, automotive braking systems, and aerospace and satellite system components.[27-30]

In the present work, we have performed a comprehensive study of the bimetallic $AlBe_n$ (n = 1–12) clusters. Besides exploring the ground state structures, we also aim to reveal the evolution of structures, stability, and various electronic structure related properties of $AlBe_n$ along with cluster size. Furthermore, we make a comparison between $AlBe_n$ and pure Be_{n+1}clusters from all aspects to analyze the Al-substitution effect. We hope that results from this study will not only offer a fundamental understanding of structure-property relationship of subnano-scale beryllium-aluminum clusters, but provide useful references for studies of other binary metal clusters.

2. Methods

The lowest-energy structures of the $AlBe_n$(n = 1–12) clusters were identified by using two methods, for both of which the spin multiplicity of 2 and 4 were taken into account. In the first one, a large number of $AlBe_n$geometries were manually built on the basis of those of pure beryllium clusters.[16] We have obtained various structures where the impurity Al atom is either attached to each possible site of the Be_n cluster or used to substitute one Be atom of the host Be_{n+1} cluster. In the second one, a stochastic search procedure[2]was used to make sure that all the global minimum structures have been found. This procedure can generate structures randomly, and hence facilitates a thorough exploration of unknown isomers. With this method, a great number of starting geometries were obtained at the B3LYP/LANL2DZ level. Afterwards, much more hunts were performed in the region of these structures to do an intensive search until no new minima appeared. Then, all the possible initial structures obtained from these two methods were optimized with subsequent frequency analysis at the B3LYP/aug-cc-pVDZ level to identify the lowest-energy ones.

To examine the energetic and electronic properties of the $AlBe_n$ clusters, single-point calculations were performed by using both B3LYP and CCSD(T) methods with the aug-cc-pVDZ basis set. Natural bond orbital (NBO) analysis[33]was carried out at the B3LYP/aug-cc-pVDZ level. At the same computational level, the spherically averaged polarizability (α) of $AlBe_n$ were calculated, which is defined as the mean value of diagonal terms of the polarizability matrix, namely,

All calculations were carried out by using the GAUSSIAN 09[34] program package. Dimensional diagrams of the molecular structures and orbitals were generated with the GaussView program.[35]

RESULTS AND DISCUSSION

3.1 Geometrical structures

First, we focus on the geometrical evolution of the $AlBe_n$(n = 1–12) clusters. To explore the Al substitution effect on beryllium clusters, the structures of Be_{n+1} were also obtained on the basis of previous reports[25,26,36] and reoptimized at the B3LYP/aug-cc-pVDZ level. The lowest-energy structures of $AlBe_n$

along with the corresponding global and local minima of the Be_{n+1} (n = 1–12) clusters are presented in Figure 1, where their spin multiplicity are also shown. It has been found that all the global minima of $AlBe_n$ are in doublet states except for $AlBe_7$ corresponding to a quartet state. The symmetry, number of Al–Be bonds, the lowest vibrational frequencies, the shortest Al-Be bond lengths, as well as the HOMO–LUMO gaps of the most stable $AlBe_n$ (n = 1–12) clusters are listed in Table 1.

The ground state structure of AlBe has a bond length of 2.439 Å and vibrational frequency of 374 cm^{-1}, according well with experimental results (R = 2.395 Å, v = 382 cm^{-1})[37]and previously reported theoretical results (R= 2.430 Å, v = 385 cm^{-1};[37] R = 2.423 Å,v = 375 cm^{-1};[38]R = 2.434 Å, v = 379.6 cm^{-1};[39]). Thus, the B3LYP/aug-cc-pVDZ treatment is considered reliable for predicting the structures of the $AlBe_n$ clusters. The global minimum of $AlBe_2$ exhibits an isosceles triangular structure with C_{2v} symmetry, in which the Al–Be and Be–Be bond lengths are 2.302 Å and 2.153 Å, respectively. Note that the Be-Be bond length of $AlBe_2$is shorter by 0.351 Å than that of Be_2, indicating that the Be–Be bond strength of Be_2 has been enhanced by the attachment of Al atom. Likewise, the Al-Be bond of $AlBe_2$is also shorter than that of AlBe.

The transition from two-dimensional (2D) to three-dimensional (3D) structures occurs at n = 3 in this series. From Figure 1, a tetrahedral configuration (C_{3v}) is obtained for $AlBe_3$, where the Al atom caps a equilateral trianglar Be_3 unit. In this structure, the Al–Be and Be–Be bond lengths are 2.324 Å and 2.048 Å, respectively. The latter is just equal to that of the lowest-energy structure of Be_4. In the case of $AlBe_4$, the most stable structure is a C_s -symmetric trigonal bipyramid with the Al atom at the top site. This structure contains two short Al–Be bonds of 2.339 Å and a long Al–Be bond of 2.721 Å.

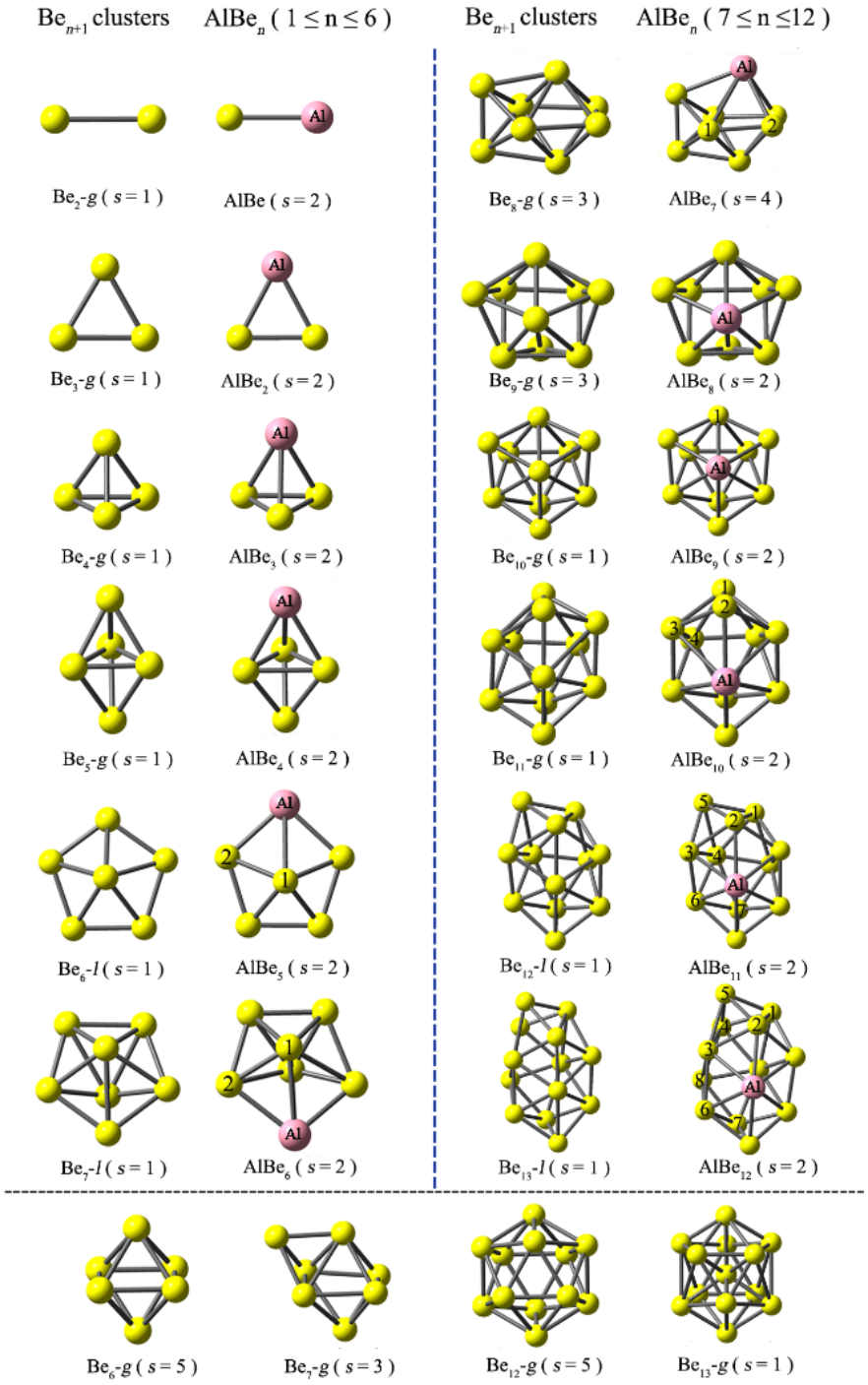

Figure 1. Ground-state geometries of the host Be$_{n+1}$clusters (1 [?] n [?] 12) on the left side. The lowest-energy structures of the AlBe$_n$ clusters (1[?] n [?] 12) on the right. In the bottom, the global minimum structures of Be$_{n+1}$ (n = 5, 6, 11, and 12) are shown. Be$_n$ -g represents a global minimum and the Be$_n$ -l represents a local minimum and the multiplicity of each structure is displayed in parentheses. Be atoms are

shown as yellow spheres while Al atoms in pink color.

It can be noticed that, from AlBe to $AlBe_4$, the larger structure can be obtained by attaching a Be atom to the smaller one. As for $AlBe_5$, the lowest-energy structure prefers a C_s -symmetric cap-like configuration, which looks similar to a metastable structure of Be_6(Be_6-l in Figure 1). The Al-Be1 and Al-Be2 bond lengths of $AlBe_5$ are 2.610 Å and 2.274 Å, respectively, and the Be–Be bond lengths vary from 1.992 Å to 2.167 Å. The lowest-lying state of $AlBe_6$ has a pentagonal bipyramidal geometry of C_2 symmetry. It can be obtained by attaching a Be atom to $AlBe_5$ from the opposite side of the Be1 atom, which accordingly shortens the Al-Be1 bond by 0.127 Å. Just like the case of $AlBe_5$, the ground state of $AlBe_6$ has a similar configuration to that of a local, but not global, minimum of Be_7. The most stable structure of $AlBe_7$ presents a bicapped octahedral structure, which can be obtained by either duplicating the Be2 atom of $AlBe_6$ or substituting an Al for the top Be atom in the global minimum of Be_8 (Be_8-g). Note that a similar structure with a spin multiplicity of 2 was also obtained for $AlBe_7$, whereas it is 4.47 kcal/mol less stable than the quartet state.

As can be seen from Figure 1, each structure of the $AlBe_n$ (n = 8-12) series could be generated by attaching a Be atom to that of $AlBe_{n-1}$. The lowest-energy structure of $AlBe_8$ can also be regarded as a result of substituting an Al atom for a Be atom in Be_9-g . A 16-faced deltahedron was identified to be the most stable structure of $AlBe_9$. Obviously, this structure can be obtained by an additional Be atom face-capping the bottom of $AlBe_8$. Meanwhile, it quite resembles the global minimum structure of Be_{10}. The ground-state structure of $AlBe_{10}$ bears strong resemblance to that of Be_{11}. It can be considered derived from $AlBe_9$ by twinning the top Be1 atom of the latter. The global minimum of $AlBe_{11}$ presents a capsule geometry derived from a local minimum structure (Be_{12}-l) of Be_{12} instead of the icosahedral Be_{12}-g . On the other hand, face-capping the $AlBe_{10}$polyhedron can also generate the structure of $AlBe_{11}$. Meanwhile, the introduction of the Be5 atom leads to lengthened Be1–Be3 distance (from 2.095 Å to 3.102 Å), so the Be1–Be3 bond is broken in $AlBe_{11}$. The most stable structure of $AlBe_{12}$ can be regarded as the result of attaching a Be (Be8) atom to $AlBe_{11}$, accompanied by broken Be4-Be6 and Be4-Be7 bonds. In this group of structures, the Al–Be bond lengths range from 2.285 Å to 2.505 Å and the Be–Be bond lengths are 2.044–2.220 Å.

Table 1. Symmetry Point Groups, the Number of Be–Al Bonds (N), the Shortest Be–Al Bond Lengths ($R_{\text{Be-Al}}$, in Å), the Lowest Vibrational Frequencies (v , in cm^{-1}), and the HOMO–LUMO Gaps (in eV) of the Lowest-energy $AlBe_n$ (n = 1–12) Clusters.

Isomers	Symmetry	N	$R_{\text{Be-Al}}$	v	gap
AlBe	$C_{[?]v}$	1	2.439	374	1.398
$AlBe_2$	C_{2v}	2	2.302	415	1.714
$AlBe_3$	C_{3v}	3	2.324	376	2.194
$AlBe_4$	C_s	3	2.339	87	1.661
$AlBe_5$	C_s	3	2.274	113	2.062
$AlBe_6$	C_2	4	2.289	67	1.482
$AlBe_7$	C_s	5	2.323	127	2.514
$AlBe_8$	C_s	5	2.285	212	2.817
$AlBe_9$	C_{3v}	6	2.362	215	2.324
$AlBe_{10}$	C_2	6	2.344	215	2.036
$AlBe_{11}$	C_1	6	2.309	203	1.758
$AlBe_{12}$	C_1	6	2.306	187	1.754

As discussed above, there is a counterpart for each lowest-energy structure of $AlBe_n$ in the minimum structures of their corresponding Be_{n+1} cluster. Besides, as can be seen in Table 1, the number of Al–Be bonds in $AlBe_n$ increases with the increasing cluster size and reaches a maximum value of six. It implies that the impurity Al atom is able to bond with six Be atoms at most. These rules may help to identify the low-lying structures of larger Al-doped Be_n clusters.

The comparison between $AlBe_n$ and other Al-doped clusters shows how the relative size of impurity atom

affects the structural evolution of the whole system. For example, the impurity Al atom always occupies an external position of the host clusters in $AlBe_n$ and AlB_n [40] until $n = 12$, while it gets trapped in the host cage from $n = 6$ onwards in $AlLi_n$ [41] and $AlNa_n$,[42,43] and from$n = 9$ onwards in the $AlTi_n$,[44]$AlSc_n$,[45]$AlPb_n$,[46] and AlY_n [47] clusters. These structural distinctions can be related to the size difference of the dopant atom versus the host atom. To be specific, the impurity Al atom (1.25 Å)[48] has larger atomic radius than those of B (0.85 Å) and Be (1.05 Å) atoms, which hinders it from entering the B_n or Be_n cages. In contrast, a framework constituted by larger host atoms such as Li (1.45 Å), Na (1.80 Å), Ti (1.40 Å), Sc (1.60 Å), Pb (1.80) and Y (1.80 Å) can accommodate the dopant Al atom.

3.2 Stability and Electronic Properties

3.2.1 Stability

The relative stability of different sized $AlBe_n$clusters can be discussed on the basis of binding energy per atom (E_b), dissociation energy (ΔE), and the second difference in energy ($\Delta^2 E$), where

These energetic properties, calculated at the CCSD(T)//B3LYP and B3LYP levels, are listed in Table S1 in supporting information. From the table, the B3LYP method overestimates binding energies and dissociation energies by 0.103–0.254 eV and 0.147–0.387 eV, respectively, when compared with the CCSD(T) results. Nevertheless, theE_b and ΔE values obtained by both methods show consistent trends. Besides, the B3LYP results of $\Delta^2 E$ accord well with those at the CCSD(T) level, and the differences are 0.033 eV–0.240 eV.

To explore the Al-substitution effect on the stability of bare beryllium clusters, the above-mentioned quantities of Be_{n+1}were also calculated according to the following equations,

For comparison, the size dependence of these energetic properties for the lowest-energy $AlBe_n$ and Be_{n+1} (n = 1–12) clusters are plotted in Figure 2. It is known that small bumps and dips in theE_b curve are indicative of relative stability and reactivity for corresponding clusters, respectively. From Figure 2a, theE_b values of $AlBe_n$ and Be_{n+1} increase sharply first, then, both curves reach a plateau from $n = 3$ to $n = 5$ and then rise again as cluster size grows. It is noted that the E_b value of an $AlBe_n$ cluster is larger by 0.033–0.324 eV than that of its corresponding Be_{n+1} cluster, suggesting that the substitution of an Al arom for a Be atom in Be_{n+1} can enhance the intracluster binding force.

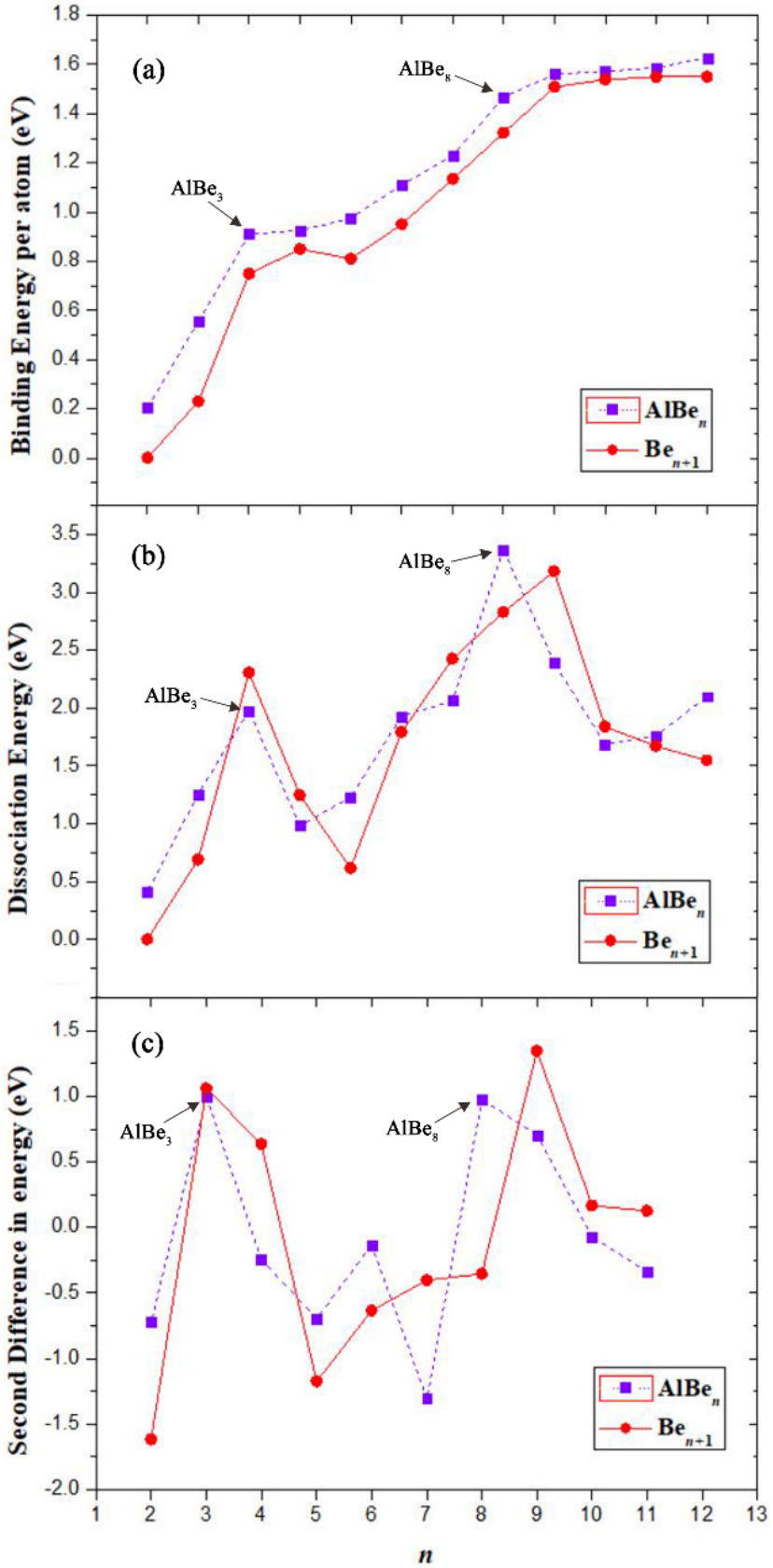

Figure 2. Size dependence of binding energies per atom (E_b), dissociation energies (ΔE), and the second difference in energy ($\Delta^2 E$) for the lowest-energy $AlBe_n$ and Be_{n+1} (n = 1–12) clusters at the CCSD(T)/aug-cc-pVDZ level.

In addition, the E_b curve of $AlBe_n$ shows two turning points at $n = 3$ and $n = 8$, indicating relatively high stability of $AlBe_3$ and $AlBe_8$. This is more clearly reflected in varying trends of ΔE and $\Delta^2 E$. As shown in Figure 2b, the ΔE curve of $AlBe_n$ has two distinct peaks at $AlBe_3$ and $AlBe_8$, indicating that these two clusters are less likely to lose a Be atom. As for Be_{n+1}, two local maximum ΔE values appear at Be_4 and Be_{10} because they are magic clusters and possess unique stability according to spherical jellium model (SJM)[15] . A similar situation can be found in the evolution of $\Delta^2 E$ values. From Figure 2c, the curves of $\Delta^2 E$ have particular peaks at $n = 3$ and$n = 8$ for $AlBe_n$, and at $n = 3$ and$n = 9$ for the Be_{n+1} series. Combining all the results given above, it can be concluded that $AlBe_3$and $AlBe_8$ have special stability among the $AlBe_n$ clusters as do Be_4 and Be_{10} in the Be_{n+1} system.

The stability of the $AlBe_n$ clusters is also examined in terms of adsorption energy of Al, *i.e.* , the energy released when an Al atom is attached to a pure Be_n cluster, which can be expressed as

The E_{ad} values of $AlBe_n$were also obtained by using the CCSD(T)//B3LYP and B3LYP methods, and the results are collected in Table S1 and plotted in Figure 3. From the figure, the two methods yield consistent results, and there are two obvious dips at $AlBe_3$ and $AlBe_8$ in both curves. These dips denote that a lot of energy is released when an Al atom is adsorbed by either Be_3 or Be_8cluster. From Table S1, all the E_{ad} values are negative, indicating that the adsoption of Al on Be_n is a favorable process. Besides, $AlBe_8$ exhibits the largest E_{ad}value (-4.132 eV at CCSD(T) level and -3.872 eV at B3LYP level), so the impurity Al atom is tightly bound to the host Be_8cluster.

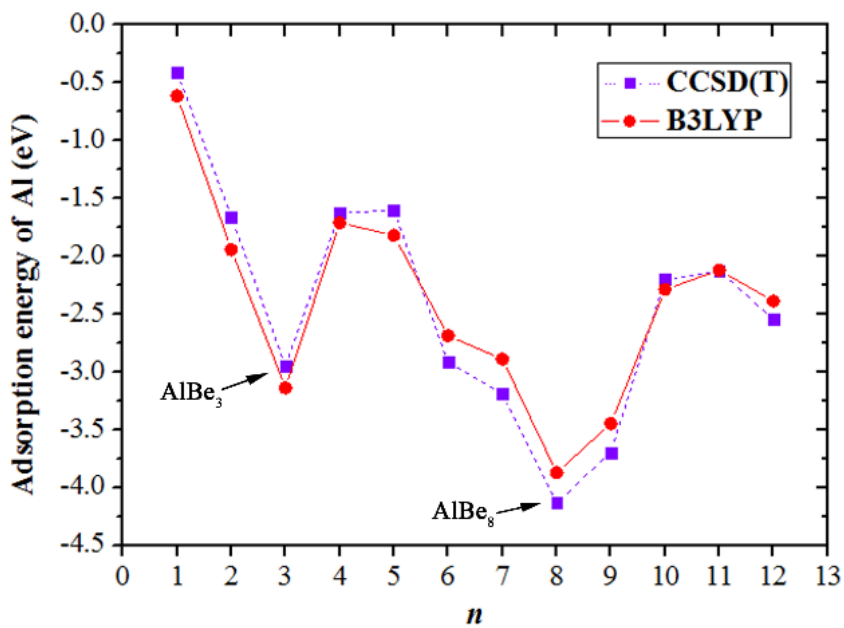

Figure 3. Size dependence of adsorption energies of Al (E_{ad}) for the lowest-energy $AlBe_n$ (n = 1–12) clusters at both CCSD(T)/aug-cc-pVDZ and B3LYP/aug-cc-pVDZ levels.

3.2.2 Electronic Properties

The stability of clusters can also be evaluated by certain electronic structure related descriptors including vertical ionization potential (*VIP*), vertical electron affinity (*VEA*), chemical hardness, the highest

occupied–lowest unoccupied molecular orbital (HOMO–LUMO) energy gap, and polarizability, etc. *VIP* is the energy difference between the ground state of the neutral cluster and the ionized cluster that has the same geometry as the neutral. In this work, the *VIP* s of the lowest-energy structures of $AlBe_n$ were calculated at the B3LYP and CCSD(T) levels. From the results shown in Figure S1a, the two curves show generally consistent trends. Either curve has two striking peaks at$n = 2$ and 8, implying that the $AlBe_2$ and $AlBe_8$ clusters are not apt to lose an electron. Meanwhile, the CCSD(T) results of $AlBe_n$ and Be_{n+1} clusters are compared in Table 2. From the table, the *VIP* value of $AlBe_n$ is always smaller than that of its corresponding Be_{n+1}cluster except for $n = 6$.

Table 2. Vertical Ionization Potential (*VIP* , in eV), Vertical Electron Affinity (*VEA* , in eV), and Hardness (η , in eV) of the Lowest-energy Be_{n+1} and $AlBe_n$ (n = 1–12) Clusters at the CCSD(T)// B3LYP/aug-cc-pVDZ Level.

3.572			
n			
1			

&& 5.995 & 0.586 &

2.705
2.683
2.338
2.516
2.169
2.341
2.288
2.159
2.293
2.156
2.032
1.889

n	Q_{Al}	NEC(Al)	NEC(Be)
1	-0.167	[core]$3s^{1.96}3p^{1.18}3d^{0.03}$	[core]$2s^{1.61}2p^{0.22}$
2	-0.621	[core]$3s^{1.90}3p^{1.66}3d^{0.05}$	[core]$2s^{1.37}2p^{0.31}$
3	-0.821	[core]$3s^{1.89}3p^{1.87}4s^{0.01}3d^{0.05}$	[core]$2s^{1.33}2p^{0.37}3s^{0.02}3p^{0.01}3d^{0.01}$
4	-0.658	[core]$3s^{1.83}3p^{1.77}3d^{0.05}$	[core]$2s^{1.30\text{-}1.43}2p^{0.37\text{-}0.53}3p^{0.01}3d^{0.01}$
5	-1.044	[core]$3s^{1.79}3p^{2.18}3d^{0.07}$	[core]$2s^{1.18\text{-}1.45}2p^{0.37\text{-}0.56}3s^{0.01}3p^{0.01}3d^{0.01\text{-}0.07}$
6	-1.435	[core]$3s^{1.76}3p^{2.56}3d^{0.10}$	[core]$2s^{1.15\text{-}1.23}2p^{0.34\text{-}0.70}3p^{0.01}3d^{0.01\text{-}0.10}$
7	-1.306	[core]$3s^{1.79}3p^{2.40}4s^{0.01}3d^{0.10}$	[core]$2s^{1.20\text{-}1.25}2p^{0.49\text{-}0.68}3p^{0.01}3d^{0.02\text{-}0.10}$
8	-1.679	[core]$3s^{1.76}3p^{2.78}4s^{0.01}3d^{0.12}$	[core]$2s^{1.18\text{-}1.31}2p^{0.42\text{-}0.68}3p^{0.01}3d^{0.02\text{-}0.04}$
9	-2.285	[core]$3s^{1.78}3p^{3.30}4s^{0.05}3d^{0.15}$	[core]$2s^{1.13\text{-}1.27}2p^{0.43\text{-}0.59}3p^{0.01\text{-}0.03}3d^{0.01\text{-}0.05}$
10	-2.403	[core]$3s^{1.73}3p^{3.48}4s^{0.04}3d^{0.15}$	[core]$2s^{1.07\text{-}1.28}2p^{0.50\text{-}0.64}3p^{0.01\text{-}0.03}3d^{0.02\text{-}0.05}$
11	-2.336	[core]$3s^{1.71}3p^{3.41}4s^{0.03}3d^{0.17}$	[core]$2s^{1.10\text{-}1.34}2p^{0.34\text{-}0.71}3p^{0.01\text{-}0.03}3d^{0.02\text{-}0.06}$
12	-2.331	[core]$3s^{1.69}3p^{3.42}4s^{0.03}3d^{0.18}$	[core]$2s^{1.07\text{-}1.37}2p^{0.31\text{-}0.76}3p^{0.01\text{-}0.03}3d^{0.02\text{-}0.05}$

can be found from Figure S2 that, the Al charge increases as the size of cluster grows and tends to flatten

out from $AlBe_9$onwards. Note that this varying trend roughly corresponds to that of coordination number of Al in the $AlBe_n$ clusters, suggesting that higher coordination number of impurity atom is beneficial to intracluster charge transfer in this case. According to Table 3, the 3s states of Al lose 0.04–0.31 electrons, while the 3p states get 0.18–2.48 electrons. As for the Be atoms, their 2s orbitals lose 0.39–0.93 electrons, while the 2p states get 0.22–0.76 electrons. Hence, the charge transfer within the $AlBe_n$clusters is mainly from the 3s orbital of Al and 2s orbitals of Be atoms to the 3p orbital of Al and 2p orbitals of Be atoms. By contrast, the contributions from other orbitals of Al and Be are negligible.

The HOMO-LUMO gaps of the $AlBe_n$ clusters at the B3LYP level are listed in Table 1 and plotted in Figure S3. From the figure, there are three obvious peaks at $AlBe_3$, $AlBe_5$ and $AlBe_8$, indicating relatively high stability of these three clusters. In particular, the $AlBe_8$ cluster possesses the largest HOMO–LUMO gap of 2.817 eV, which not only is larger than the experimental gap value of 1.9 eV for the kinetically stable C_{60},[47] but also exceeds that of 2.53 eV (computed at the same level) for the chemically inert superatom Al_{13}^-.[48] For comparison, the HOMO–LUMO gaps of the Be_{n+1}clusters are also depicted in Figure S3. It can be found that substituting an Al atom for a Be atom enlarges the HOMO–LUMO gaps of Be_8 and Be_{10} clusters by 0.689 eV and 0.398 eV, respectively, while the Al substitution effect is insignificant for Be_{11} and Be_{13} clusters and is negative for the other beryllium clusters.

Finally, the evolution of polarizability per atom of $AlBe_n$ (n = 1–12) is considered since the static polarizability is an important measure of electronic properties of clusters. From the results shown in Figure 4, a turning point at$n = 3$ can be found, which squares with the geometry transformation from planar to steroescopic at $AlBe_3$. For comparison, the polarizability per atom of the lowest-energy Be_{n+1} clusters are also given in Figure 4. From the figure, both curves show generally decreasing trends with increasing cluster size, and gradually become stable for larger sizes. Besides, substituting a Be atom in Be_{n+1} with an Al atom always brings about a larger polarizability to the doped cluster, although the Al-substitution effect is less prominent for larger-sized ones. Hence, the $AlBe_n$ clusters are more polarizable compared with their corresponding Be_{n+1} clusters. Note that there is a relatively large polarizability gap between Be_6 and $AlBe_5$, which can be attributed to the large structural discrepancy between these two clusters since polarizability is sensitive to the shape of the system.[50]

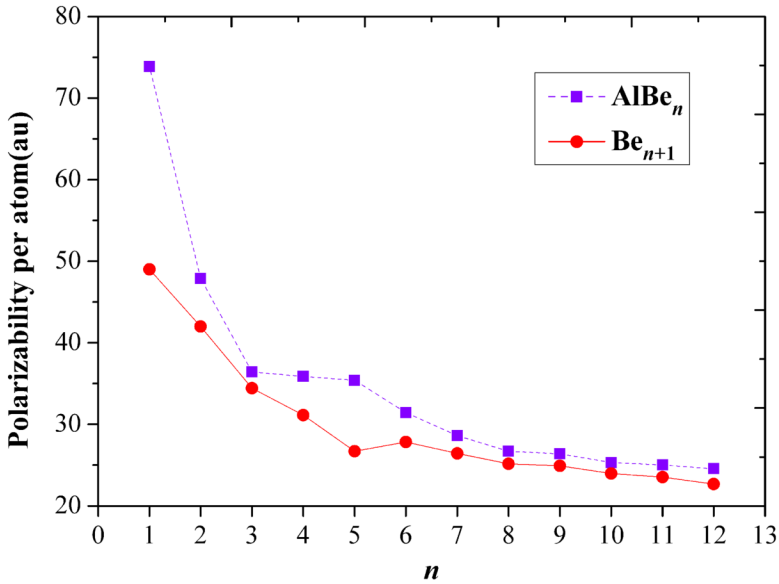

Figure 4. Size dependence of polarizabilities per atom for the lowest-energy $AlBe_n$ and Be_{n+1} (n = 1–12)

clusters at the B3LYP/aug-cc-pVDZ level.

3.3 In-depth study of $AlBe_3$ and $AlBe_8$

Based on the preceding analysis of energetic and electronic properties, it is interesting to find that the $AlBe_3$ and $AlBe_8$ clusters possess special stability among the $AlBe_n$ series. Hence, the electronic structure and density of states (DOS) of these two clusters are further investigated. To facilitate comparison, the total and partial density of states (TDOS and PDOS) of $AlBe_3$ and $AlBe_8$ as well as their corresponding Be_4 and Be_9 clusters are plotted as a function of energy in Figure 5, in which their valence molecular orbitals (MOs) obtained at the ROMP2//B3LYP level are also illustrated.

From Figure 5b, the singly-occupied HOMO orbital of $AlBe_3$ exhibits dominant s state, the HOMO-1 to HOMO-3 orbitals present typical p shape, and the HOMO-4 orbital shows spherically symmetric s character. So the valence electron configuration of $AlBe_3$ is $1S^{\,2}1P^{\,6}2S^{\,1}$. As for the $AlBe_8$ cluster, its nineteen valence electrons are arranged in the $1S^{\,2}1P^{\,6}1D^{\,10}2S^{\,1}$ pattern, which accords well with the prediction of the spherical jellium model.[15] Compared with $AlBe_8$, the triplet Be_9 cluster is one D electron less and has a electronic shell structure of $1S^{\,2}1P^{\,6}1D^{\,9}2S^{\,1}$ (see Figure 5c). As the studied $AlBe_n$ clusters are all open-shell species, there are not any shell-closed magic clusters in this series. However, the $AlBe_3$ and $AlBe_8$ clusters do exhibit enhanced stability relative to their congeners. A possible explanation is that both of them are one electron short of shell closure, and their desire for an additional electron makes the component atoms bind so tightly with each other that the clusters are stable against dissociation of any kind.

From Figure 5, the introduction of Al impurity has more effect on the DOS of p-type molecular orbitals of beryllium clusters. The comparison between TDOS of Be_4 and $AlBe_3$ shows that the peak near -6 eV for the former splits into two peaks in the latter. Similarly, the peak around -9.5 eV in the TDOS plot of Be_9 also splits into two peaks at -9.5 eV and -10 eV in that of $AlBe_8$. In contrast, the Al doping effect is minor on the DOS of other states.

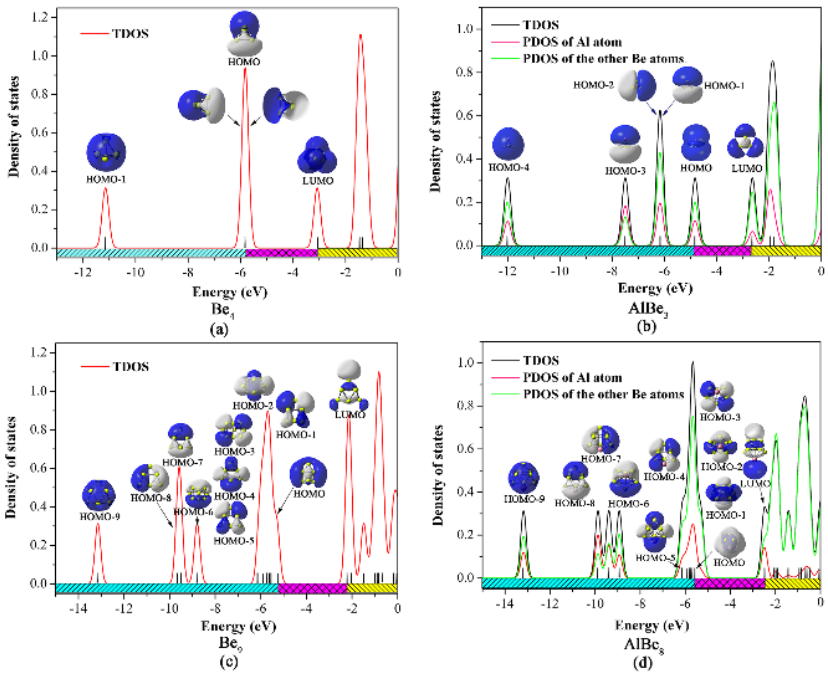

Figure 5. Density of states (DOS) and valence molecular orbitals (shown as insets) of the $AlBe_3$, $AlBe_8$, Be_4, and Be_9clusters.

Conclusions

The structures, relative stability, and electronic properties of the lowest-energy $AlBe_n$ (n = 1–12) clusters were systematically studied by high-level *ab initio* and density functional theories. The geometry transformation from planar to steroescopic occurs at $AlBe_3$ in this series. The impurity Al atom prefers to reside ouside the host Be_n cluster until $n = 12$ and only slightly affects the configuration of the latter. NBO analysis reveals that 0.167˜2.403|e| charge flows from the host Be_n to the Al atom, which might be due to the larger electronegativity of Al than Be. The evolutions ofE_b , $\Delta^2 E$, ΔE ,E_{ad}, and HOMO-LUMO gap with cluster size show special stability of $AlBe_3$ and $AlBe_8$among the $AlBe_n$ clusters. Moreover, a comparison has been made between $AlBe_n$ and pure beryllium clusters, and it is found that substituting an Al atom for a Be atom in Be_{n+1} results in enhanced binding energy and polarizability but decreased chemical hardness of the system.

Acknowledgments

This work was supported by the National Natural Science Foundation of China (Grant No. 21573089, 51872057, 21603032), the "13th Five-Year" Science and Technology Research Project of Jilin provincial education department (JJKH20190117KJ), Natural Science Foundation of Fujian Province (Grant No. 2016J05032, 2016J01771), and MiaoPu Foundation of Fujian Medical University (2015MP034).

Keywords:doped cluster, Be-Al alloy, bimetallic, optimization, stability

References and Notes

1. X. Li, A. E. Kuznetsov, H.-F. Zhang, A. I. Boldyrev, L.-S. Wang,*Science* , **2001** , 291, 859-861.
2. O. Thomas, W. Zheng, S. Xu, K. Bowen, *Phys. Rev. Lett.***2002** , 89.213403.
3. D. E. Bergeron, A. W. Castleman, T. Morisato, S. N. Khanna,*Science* , **2004** , 304, 84-87.
4. D. E. Bergeron, P. J. Roach, A. W. Castleman, N. O. Jones, S. N. Khanna, *Science* , **2005** , 307, 231-235.
5. A. I. Boldyrev, L.-S. Wang, *Chem. Rev.* **2005** , 105, 3716-3757.
6. L. Cheng, K. Xiao-Yu, L. Zhi-Wen, M. Ai-Jie, M. Yan-Ming, *J. Phys. Chem. A* . **2011** , 115, 9273-9281.
7. Z. Luo, C. J. Grover, A. C. Reber, S. N. Khanna, A. W. Castleman, Jr.,*J. Am. Chem. Soc.* **2013** , 135, 4307-4313.
8. R. Burgert, H. Schnockel, A. Grubisic, X. Li, S. T. Stokes, K. H. Bowen, G. F. Gantefor, B. Kiran, P. Jena, *Science* ,**2008** , 319, 438-442.
9. P. J. Roach, W. H. Woodward, A. W. C. Jr., A. C. Reber, S. N. Khanna,*Science* , **2009** , 323.
10. S. A. Claridge, J. A. W. Castleman, Shiv N. Khanna, C. B. Murray, A. Sen, P. S. Weiss, *ACS Nano* , **2009** , 3, 244–255.
11. J. A. W. Castleman, S. N. Khanna, *J. Phys. Chem. C* .**2009** , 113, 2664–2675.
12. M. Qian, A. C. Reber, A. Ugrinov, N. K. Chaki, S. Mandal, Hector M. Saavedra, S. N. Khanna, A. Sen, P. S. Weiss, *ACS Nano* ,**2010** , 4, 235–240.
13. N. K. Chaki, S. Mandal, A. C. Reber, M. Qian, H. M. Saavedra, P. S. Weiss, S. N. Khanna, A. Sen, *ACS Nano* , **2010** , 4 5813–5818.
14. S. Mandal, A. C. Reber, M. Qian, P. S. Weiss, S. N. Khanna, A. Sen,*Acc. Chem. Res.* **2013** .
15. (a) W. D. Knight, K. Clemenger, W. A. d. Heer, A.Saunders, *Phys. Rev. Lett.* 1984. 52, 2141-2143. (b) W. Ekardt, *Phys. Rev. B* .**1984** , 29, 1558-1564.
16. Baltenkov A S, Manson S T, Msezane A Z, *J. Phys. B: At. Mol. Opt. Phys.* **2015** , 48(18): 185103.
17. Varas A, García-González P, Feist J, et al. Quantum plasmonics: from jellium models to ab initio calculations[J]. Nanophotonics,**2016** .
18. V. E. Bondybey, *Chem. Phys. Lett.* **1984** , 109, 436-441.
19. J. Stärck, W. Meyer, *Chem. Phys. Lett.* **1996** , 258, 421-426.
20. J. M. L. Martin, *Chem. Phys. Lett.* 1999, 303, 399–407.
21. K. Patkowski, V. Spirko, K. Szalewicz, *Science* , **2009** , 326, 1382-1384.
22. J. M. Merritt, V. E. Bondybey, M. C. Heaven, *Science* , 2009, 324, 1548-1551.

23. D. R. Lide, ed., CRC Handbook of Chemistry and Physics, CRC Press, Boca Raton, **2008** . 89th.
24. M. C. Heaven, J. M. Merritt, V. E. Bondybey, Annu. *Rev. Phys. Chem.* **2011** , 62, 375-393.
25. J. Wang, G. Wang, J. Zhao, *J. Phys.: Condens. Mat.***2001** , 13, 753–758.
26. V. Cerowski, B. K. Rao, S. N. Khanna, P. Jena, S. Ishii, K. Ohno, Y. Kawazoe, *J. Chem. Phys.* **2005** , 123, 074329.
27. Parsonage T. *Mater. Sci. tech.* **2000** , 16(7-8): 732-738.
28. Schuster G, Pokross C, *Light Metals.* **2013** , 2013: 259-264.
29. Sweeney M, Acreman M, Vettese T, Application and testing of additive manufacturing for mirrors and precision structures[C].**2015** : 957406-957406-13.
30. Previtali B. Metal Matrix Composites: Casting Processes[J]. Wiley Encyclopedia of Composites, **2012** .
31. J. Tong, Y. Li, D. Wu, Z.-R. Li, X.-R. Huang, *J. Chem. Phys.***2009** , 131, 164307.
32. M. Saunders, *J. Comput. Chem.* **2004** , 25, 621-626.
33. E. D. Glendening, A. E. Reed, J. E. Carpenter, F. Weinhold, NBO Version 3.1, Theoretical Chemistry Institute, University of Wisconsin, Madison, 1996.
34. M. J. Frisch, H. B. Schlegel, G. E. Scuseria, , J. R. C. M. A. Robb, G. Scalmani, V. Barone, B. Mennucci, , H. N. G. A. Petersson, M. Caricato, X. Li, H. P. Hratchian, , J. B. A. F. Izmaylov, G. Zheng, J. L. Sonnenberg, M. Hada, , K. T. M. Ehara, R. Fukuda, J. Hasegawa, M. Ishida, T. Nakajima, , O. K. Y. Honda, H. Nakai, T. Vreven, J. A. Montgomery, Jr., , F. O. J. E. Peralta, M. Bearpark, J. J. Heyd, E. Brothers, , V. N. S. K. N. Kudin, R. Kobayashi, J. Normand, , A. R. K. Raghavachari, J. C. Burant, S. S. Iyengar, J. Tomasi, , N. R. M. Cossi, J. M. Millam, M. Klene, J. E. Knox, J. B. Cross, , C. A. V. Bakken, J. Jaramillo, R. Gomperts, R. E. Stratmann, , A. J. A. O. Yazyev, R. Cammi, C. Pomelli, J. W. Ochterski, , K. M. R. L. Martin, V. G. Zakrzewski, G. A. Voth, , J. J. D. P. Salvador, S. Dapprich, A. D. Daniels, , J. B. F. O. Farkas, J. V. Ortiz, J. Cioslowski, and D. J. Fox, Gaussian 09, Revision A.01, Gaussian, Inc., Wallingford CT,**2009** .
35. R. Dennington, T. Keith, J. Millam, GaussView, Version 5, Semichem, Inc., Shawnee Mission, KS, **2009** .
36. S. Srinivas and J. Jellinek, *J. Chem. Phys.* , **2004** , 121, 7243.
37. J. M. Merritt, V. E. Bondybey, M. C. Heaven, *Phys. Chem. Chem. Phys.* **2008** , 10, 5403.
38. VW Ribas, LT Ueno, O Roberto-Neto, *Chem. Phys.* **2006** , 330(1): 295-300.
39. J Wang, D Zhai, F Guo, *Theor. Chem. Acc.* **2008** , 121(3-4): 165-172.
40. X.-J. Feng, Y.-H. Luo, *J. Phys. Chem. A.* **2007** , 111, 2420-2425.
41. H.-P. Cheng, R. Barnett, U. Landman, *Phys. Rev. B* .**1993** , 48, 1820-1824.
42. A. Dhavale, V. Shah, D. G. Kanhere, *Phys. Rev. A* .**1998** , 57, 4522-4527.
43. R. Zope, S. Blundell, C. Guet, T. Baruah, D. Kanhere, *Phys. Rev. A* . **2001** , 63.043202.
44. J. Xiang, S. H. Wei, X. H. Yan, J. Q. You, Y. L. Mao, *J.Chem. Phys.* **2004** , 120, 4251.
45. M. Wang, G. Qiu, X. Huang, Z. Du, Y. Li, *J. Phy.: Condens. Mat.***2009** , 21, 046004.
46. D.-L. Chen, W. Tian, C.-C. Sun, *Phys. Rev. A* . **2007** , 75. 013201.
47. G.-f. Zhao, J. Zhang, Q. Jing, Y.-h. Luo, Y.-x. Wang, *J. Chem. Phys.* **2007** , 127, 234312.
48. J. C. Slater, *J. Chem. Phys.* **1964** , 41, 3199.
49. R. G. Parr, R. G. Pearson, *J. Am. Chem. Soc.* **1983** , 105, 7512–7516.
50. W. D. Knight, K. Clemenger, W. A. de Heer, W. A. Saunders, *Phys. Rev. B* . 31, 2539 (**1985**).